IEEE Access
Multidisciplinary | Rapid Review | Open Access Journal

Received 14 September 2022, accepted 2 October 2022, date of publication 5 October 2022, date of current version 12 October 2022.

Digital Object Identifier 10.1109/ACCESS.2022.3212155

RESEARCH ARTICLE

Optimization of Torque Control Parameters for Wind Turbine Based on Drive Chain Active Damping Control

YINGMING LIU[1], SHUYUAN ZHANG[1], XIAODONG WANG[1], XING GAO[1], AND TIAN CAO[2]
[1]School of Electrical Engineering, Shenyang University of Technology, Shenyang 110000, China
[2]School of Electrical Engineering, China University of Mining and Technology, Xuzhou 221000, China

Corresponding author: Shuyuan Zhang (572280373@qq.com)

This work was supported by the National Natural Science Foundation of China under Grant 51677121.

ABSTRACT Considering the mutual coupling effect of wind turbine control parameters, an optimization method of the control parameters for torque system based on drive chain active damping control is proposed, which improves the control accuracy and solves the problem that the control objectives are difficult to coordinate. Firstly, the mathematical model of the torque-speed system and the dynamical model of the drive chain active damping control are established. At the same time, the initial value of active damping gain is calculated according to the designed band-pass filter measurement results. Secondly, to facilitate the setting of proportional-integral (PI) control parameters, the Routh method is adopted to identify the torque-speed system with large inertia characteristic as a low-order inertia system. Subsequently, the Integrated Time and Absolute Error (ITAE) criterion is used to set the initial value of the PI control parameters for the torque system. Furthermore, the PI control parameters and active damping gains at each equilibrium point are optimized based on the Hierarchic Genetic Algorithm, which improves the accuracy of control parameters. At the same time, the control objectives are coordinated by optimizing weight allocation based on the Pareto. Then the adaptive control method is constructed by fitting them with the wind speed to improve the control accuracy far from the equilibrium points. Finally, the effectiveness of the proposed method is verified by comparing the frequency-domain characteristic, control accuracy, twist vibration of the drive chain, tower vibration and load.

INDEX TERMS Torque control, drive chain active damping control, system identification, control parameters optimization, hierarchic genetic algorithm.

I. INTRODUCTION

Nowadays, mature proportional-integral (PI) control is still widely used in traditional torque control for wind turbines to adjust the generator torque [1], [2], which has a simple design structure, high stability, and can realize the rapid adjustment of parameters. Compared with other new control strategies that have not been widely applied in engineering, the research on PI control will not stay at the theoretical level and have broad application prospects in future practical engineering. However, during the torque control action, the difference between aerodynamic and electromagnetic torque leads to severe twist vibration of the drive chain, which will further aggravate the side-side vibration and y-direction load of the tower. Therefore, additional active damping control of the drive chain is required [3], [4]. At the same time, the problems of inaccurate control parameters and the difficulty in coordinating control objectives need to be solved urgently [5], [6]. From the above analysis, it is valuable and significant to research the optimization method of torque system control parameters based on drive chain active damping control.

In response to the above problems, scholars worldwide have conducted excellent research on optimizing torque control parameters of wind turbines. On the one hand, the method of setting PI control parameters of the torque system through frequency-domain characteristic is still widely used. A setting

The associate editor coordinating the review of this manuscript and approving it for publication was Huaqing Li.

method of the PI control parameters is proposed in [7], but the influence of the accuracy of system identification on the setting result is not considered. On the other hand, the method of using active damping control to suppress the drive chain twist vibration has attracted extensive attention. The active damping control of the drive chain is added to the traditional torque system. Since there is no explicit equation calculation and optimization method for active damping gain, the control effect of this method is not ideal [8], [9]. The universality of the intelligent algorithm to optimize control parameters has gradually become a hot research topic in recent years. This method is based on an intelligent algorithm, but the intercoupling effect of multiple control parameters leads to control parameters inaccuracy and control objectives difficult to coordinate [10], [11]. In addition, many simulation results are required to calculate the weighting relationships between multiple parameters according to an orthogonal experiment method, which will seriously affect the research efficiency [12]. In [13] and [14], the PI control parameters are optimized based on the genetic and particle swarm optimization algorithms. However, the poor population diversity in the later stage of the genetic algorithm influences the optimization results. Moreover, the insufficient convergence of the particle swarm optimization algorithm leads to the poor efficiency of the algorithm. In addition, scholars worldwide have been widely concerned with adaptive control strategy in the last several years. However, the variable gain control established has an error when switching control parameters [15]. Moreover, the constant or discrete drive chain active damping gain cannot always retain the optimal control state [16].

In order to solve the above problems, considering the mutual coupling of the wind turbine control parameters, an optimization method of torque system control parameters based on drive chain active damping control is proposed in this paper, which improves the control accuracy and solves the problem that the control objectives are difficult to coordinate. Based on this, the main contributions of this paper can be concluded as follows.

(1) The Hierarchic Genetic Algorithm (HGA) with multiple subpopulations is proposed to optimize the control parameters of the wind turbine, which can effectively maintain population diversity and overcome the problem of premature convergence. Furthermore, the proposed method can also improve the accuracy of control parameters.

(2) The Pareto method is proposed to coordinate wind turbine control objectives by optimizing weight allocation, which can reduce the load while improving the control accuracy.

(3) The adaptive control method of control parameters is proposed, which solves the problem that constant or discrete control parameters cannot always maintain the best control effect far from the equilibrium points.

The main advantages of the proposed method include the following aspects. In the first aspect, the control parameter optimization method based on the HGA can improve the accuracy of control parameters. In the second aspect, the weight allocation optimization method based on the Pareto can coordinate the control objectives. In the third aspect, the proposed adaptive control method can improve the control accuracy far from the equilibrium points. However, the disadvantage of the proposed method is poor applicability under transient wind conditions. Therefore, real-time online optimization is needed when extreme weather condition occurs.

The rest of this paper is organized as follows. In section II, the mathematical model of the torque-speed system and the dynamical model of the drive chain active damping control are established. Furthermore, the active damping gain initial value is calculated. In section III, the Routh method is adopted to identify the torque-speed system as a low-order inertial system, and the ITAE is used to set the initial values of PI control parameters for the torque system. In section IV, an optimization method of PI control parameters for torque system and active damping gain based on Pareto and HGA is proposed. Moreover, an adaptive control method far from the equilibrium point is proposed. In section V, the proposed method is verified by simulation results in the frequency domain and time domain. In section VI, the conclusions and future research directions are drawn.

II. MATHEMATICAL MODEL OF TORQUE-SPEED SYSTEM AND DYNAMIC MODEL OF DRIVE CHAIN ACTIVE DAMPING CONTROL

The traditional PI control is widely used in the torque control strategy of wind turbines. The net difference $\Delta\omega$ between the rated value ω_{rated} of the generator speed and the measured value $\omega_{measure}$ is controlled by the torque system PI control to output a rated generator torque T_{rated}. However, since the modal damping of the drive chain is small, the twist vibration of the drive chain is easily caused by the difference between the aerodynamic and the electromagnetic torque. In addition, the twist vibration of the drive chain will also aggravate the side-side vibration of the tower top and the y-direction load of the tower bottom. Therefore, based on the traditional torque control, it is necessary to add the active damping control of the drive chain to enhance its equivalent modal damping. However, it is not easy to measure the twist rate $d\gamma/dt$ the drive chain. Generally, the value $d\gamma/dt$ of the drive chain twist rate can be obtained based on the measured value $\omega_{measure}$ of the generator speed through a band-pass filter (BPF). Then, with the active damping gain H_c, the additional generator torque T_{ad} is obtained. At this time, the given generator torque T of the torque-speed system is composed of the rated generator torque T_{rated} of the traditional torque control and the additional generator torque T_{ad} of the drive chain active damping control. The diagram of wind turbine control is shown in Figure 1.

In this paper, the physical simulation example based on Bladed software is built according to the actual parameters of the 2MW wind turbine. The main parameter values of the 2MW wind turbine are shown in Table 1.

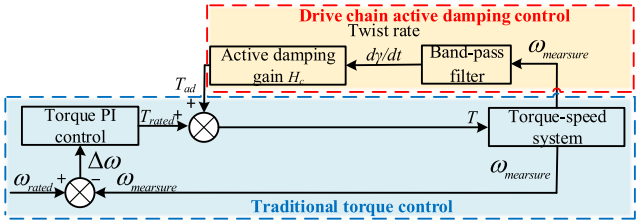

FIGURE 1. Diagram of wind turbine control.

TABLE 1. Main parameter value of the 2MW wind turbine.

Main parameter name	Main parameter value
Generator rated speed	1500 r/min
Drive chain damping ratio	0.015
Drive chain resonance frequency	2.52 Hz
Wind speed range	4 m/s~25 m/s
Rated wind speed	11 m/s
Torque control range	9 m/s~11 m/s
...	...

A. MATHEMATICAL MODEL OF TORQUE-SPEED SYSTEM

In this paper, the wind turbine equilibrium points are wind speed points of 9 m/s, 9.5 m/s, 10 m/s, 10.5 m/s, and 11 m/s. Therefore, the other wind speed points in the torque control range (9 m/s~11 m/s) with a step of 0.1 are defined as far from the equilibrium points. Based on the 2MW wind turbine, the mathematical models of the torque-speed system will be established in this section.

The wind turbine is a strong nonlinear system. In order to obtain the linearized model of the wind turbine, the Taylor series expansion method is adopted to linearize each equilibrium point. Therefore, the nonlinear wind turbine can be transformed into a multiple-input multiple-output (MIMO) state space equation, which is shown in equation (1). At the equilibrium points, the linear system mathematical model obtained by linearization is the same as the nonlinear wind turbine model [17].

$$\begin{cases} \dot{x} = Ax + Bu \\ y = Cx + Du \end{cases} \tag{1}$$

In equation (1), A, B, C, and D denote three-dimensional coefficient matrices, x denotes the state variable, u and y denote the input variable and output variable, respectively. Please refer to Appendix I for further details.

Moreover, the wind turbine is a parameter time-varying system. In order to obtain a single input single output (SISO) system with a constant wind speed of the wind turbine, the wind speed, input, and output of the above MIMO system are extracted [18]. When the wind speed is 10m/s, the torque-speed system $G_{10}(s)$ of the wind turbine can be expressed as:

$$\begin{aligned} G_{10}(s) = -[&0.016673(s^2 + 0.04387s + 8.52)(s^2 + 0.1552s \\ &+ 20.87)(s^2 + 9.724s + 378.4)(s^2 + 0.729s \\ &+ 449.1)(s^2 + 0.628s + 558.4)][(s + 0.06913)(s^2 \\ &+ 0.03167s + 8.88)(s^2 + 2.167s + 199.3)(s^2 \\ &+ 5.227s + 447.5)(s^2 + 1.331s + 525.2)(s^2 \\ &+ 2.525s + 633)] \end{aligned} \tag{2}$$

Based on the above methods, the mathematical models of the torque-speed systems at the other equilibrium points for the 2MW wind turbine can be established.

B. DYNAMIC MODEL OF DRIVE CHAIN ACTIVE DAMPING CONTROL

The drive chain is composed of a low-speed shaft, gearbox, and high-speed shaft, whose typical simplified structure is shown in Figure 2, where K_c denotes the stiffness of the drive chain, D_c denotes the damping of the drive chain, J_r denotes the rotational inertia of the wind wheel, J_g denotes the rotational inertia of the generator, ω_r denotes the rotor speed of the wind wheel, ω_g denotes the generator rotor speed, T_a denotes aerodynamic torque of the wind wheel, T_e denotes electromagnetic torque of the generator.

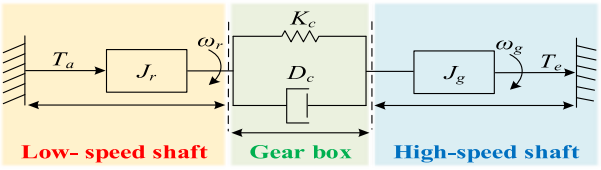

FIGURE 2. Simplified drive chain structure.

According to Figure 2, the torque transmission process can be linearized as follows [19].

$$\begin{cases} J_r \dfrac{d\omega_r}{dt} = T_a - K_c\gamma - D_c\dfrac{d\gamma}{dt} \\ J_g \dfrac{d\omega_g}{dt} = K_c\gamma + D_c\dfrac{d\gamma}{dt} - T_e \end{cases} \tag{3}$$

where, γ denotes the twist angle of the drive chain, $d\gamma/dt$ denotes the twist rate of the drive chain.

In equation (3), the drive chain twist angle γ and drive chain twist rate $d\gamma/dt$ can be defined as:

$$\gamma = \int (\omega_r - \omega_g)dt \tag{4}$$

$$\frac{d\gamma}{dt} = \omega_r - \omega_g \tag{5}$$

If additional torque T_{ad}, which is opposite to the twist rate of the drive chain, is added to the electromagnetic torque T_e of the generator, it can be expressed as:

$$T_{ad} = -H_c\frac{d\gamma}{dt} \tag{6}$$

where, H_c denotes the active damping gain of the drive chain.

From equation (3) and (6), it can be deduced:

$$\begin{aligned} J_g\frac{d\omega_g}{dt} &= K_c\gamma + D_c\frac{d\gamma}{dt} - (T_e + T_{ad}) \\ &= K_c\gamma + (D_c + H_c)\frac{d\gamma}{dt} - T_e \end{aligned} \tag{7}$$

According to equation (7), it can be proved that the active damping control of the drive chain can increase its equivalent damping from D_c to $(D_c + H_c)$ after adding additional torque T_{ad}.

According to equation (6), the twist rate of the drive chain is needed to calculate the active damping gain H_c of the drive chain. However, it is not easy to measure the twist rate $d\gamma/dt$ of the drive chain. Generally, the value of the drive chain twist rate can be obtained based on the measured value of the generator speed through a BPF. The transfer function of BPF can be expressed as:

$$G_{filter}(s) = \frac{2\xi\omega_0 s}{s^2 + 2\xi\omega_0 s + \omega_0^2} \tag{8}$$

where, ξ denotes the damping ratio of BPF, ω_0 denotes the center frequency of BPF.

With the measured value of the generator speed as an input variable into the BPF, the output of the BPF is the value of the drive chain twist rate. The drive chain damping ratio is selected as the value of the BPF damping ratio [20]. To suppress the twist vibration of the drive train, the frequency of the additional torque provided by active damping control needs to be at the drive train resonance frequency [21]. According to equation (6), since the additional torque is generated by the drive chain twist rate, the frequency of the drive chain twist rate output by the BPF needs to be at the drive chain resonance frequency. Therefore, the drive chain resonance frequency is selected as the value of the BPF center frequency [22]. The damping ratio and resonance frequency of the drive chain in the 2MW wind turbine can be obtained by Campbell analysis, as shown in Figure 3 and 4.

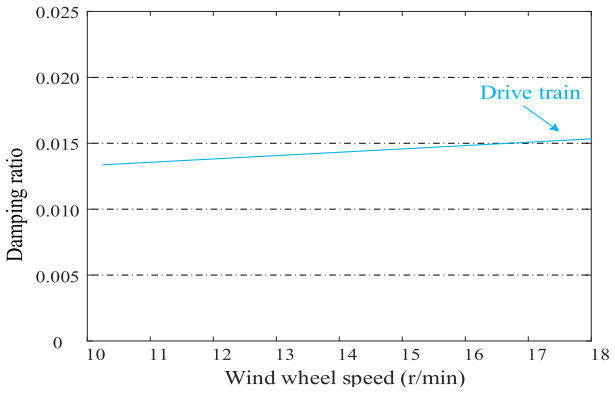

FIGURE 3. Drive chain damping ratio obtained by Campbell.

It can be observed from Figure 3 and 4 that the damping ratio of the drive chain is near 0.015, and the resonance frequency of the drive chain is near 2.52 Hz. In the torque control, the wind wheel speed range is 16∼18 r/min. Therefore, the damping ratio and center frequency of the designed BPF are selected at 0.015 and 2.52 Hz. The Bode plot of the designed BPF is shown in Figure 5.

The above parameters are from the built 2MW wind turbine. In order to prevent secondary disasters of shafting,

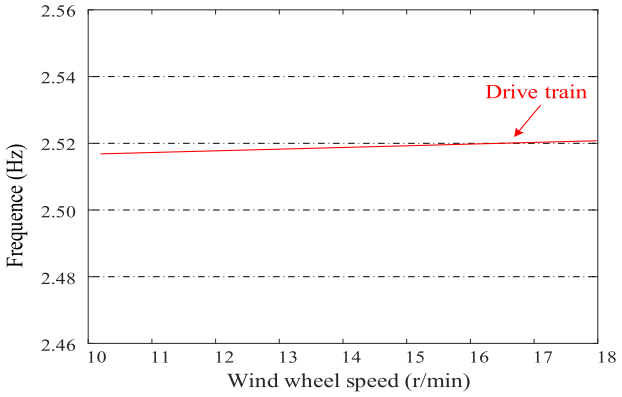

FIGURE 4. Drive chain resonance frequency obtained by Campbell.

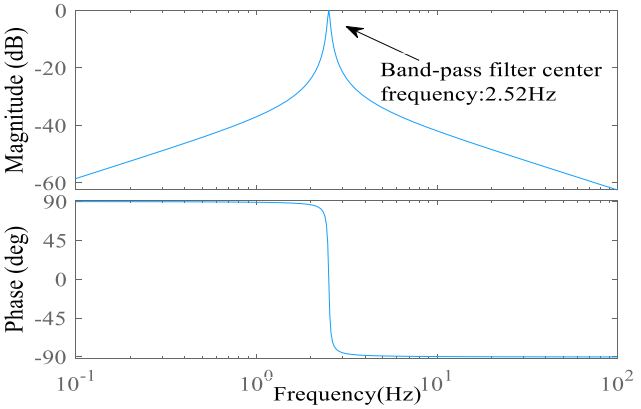

FIGURE 5. Bode plot of the designed BPF.

10% of the maximum torque of the generator is selected for additional torque. Under torque control, the average value of the BPF output is selected as the twist rate of the drive train. Thereby, the initial value H_c of the active damping gain is calculated.

III. TORQUE-SPEED SYSTEM IDENTIFICATION AND PI CONTROL PARAMETERS OF TORQUE SYSTEM SETTING

A. TORQUE-SPEED SYSTEM IDENTIFICATION

In order to facilitate the setting of the initial value of PI control parameters, the torque-speed system $G_{10}(s)$ with large inertia characteristic is identified as a low-order inertia system by using the Pade and Routh methods. The Routh method is selected in this paper because of its excellent stability and high fitting accuracy [23]. For the Routh method, the transfer function is expanded into the forms of equation (9) and (10) and then identified as a low-order inertial system according to the Routh table:

$$G(s) = \sum_{i=1}^{n} \beta_i \prod_{j=1}^{i} F_j(s) \tag{9}$$

$$F_j(s) = \frac{1}{a_j s + \cfrac{1}{a_{j+1}s + \cfrac{1}{\ddots_{a_{n-1}s + \frac{1}{a_n s}}}}} \tag{10}$$

where, a_i and β_i can be obtained directly from the Routh table.

Based on the Pade and Routh methods, equation (2) is identified as a low-order inertial system. Therefore, the low-order inertial systems $G_{10\_Pade}(s)$ and $G_{10\_Routh}(s)$ are expressed in equation (11) and (12), respectively. The open-loop step response compared with the torque-speed system is shown in Figure 6.

$$G_{10\_Pade}(s) = \frac{-0.004456s^2 - 0.002845s - 0.06917}{s^3 + 2.187s^2 + 64.72s + 4.483} \tag{11}$$

$$G_{10\_Routh}(s) = \frac{-0.004435s^2 - 0.002837s - 0.06915}{s^3 + 2.186s^2 + 64.89s + 4.476} \tag{12}$$

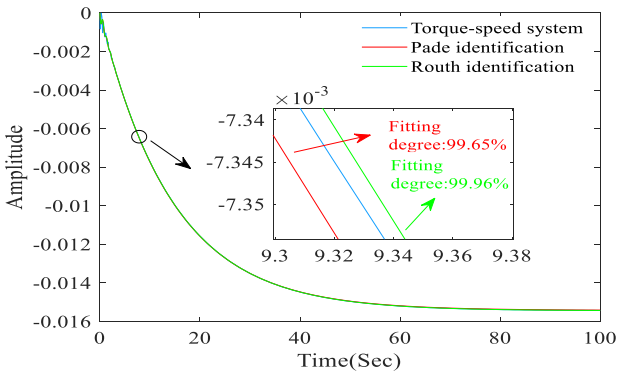

FIGURE 6. Open-loop step response comparison curves.

According to the above analysis, the Pade and Routh methods can comprehensively reflect the characteristic of torque-speed system $G_{10}(s)$. The fitting degree of the Pade and Routh methods reaches 99.73% and 99.94%, respectively. Therefore, with higher accuracy, $G_{10}(s)$ is identified as $G_{10\_Routh}(s)$ by the Routh method.

B. PI CONTROL PARAMETERS OF TORQUE SYSTEM SETTING

$G_{10\_Routh}(s)$ is the controlled system. In order to obtain the PI control parameters of the torque system with high accuracy, the Integral of Timed and Square Error (ITSE) and Integrated Time and Absolute Error (ITAE) criteria are used to set the PI control parameters initial value of the torque system [24]. The error integration criteria are shown in Table 2.

TABLE 2. Error integral criterion index.

Criterion index	Form
ITSE	$\int_0^\infty te^2(t)dt$
ITAE	$\int_0^\infty t\|e(t)\|dt$

where, t denotes the time, $e(t)$ denotes the error function.

The initial value of PI control parameters for the torque system is set based on the ITSE and ITAE criteria. The closed-loop step response comparison curves are shown in Figure 7.

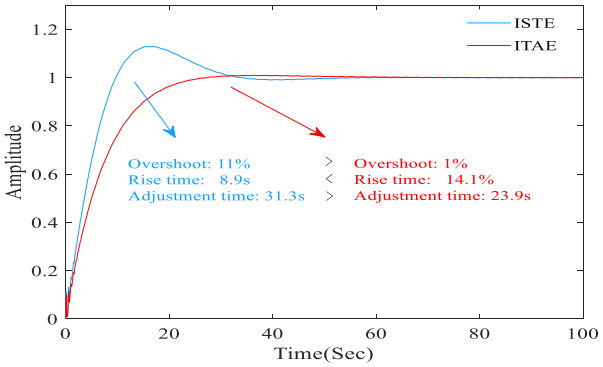

FIGURE 7. Closed-loop step response comparison curves.

According to the analysis, the PI control parameters of the torque system calculated by ITSE and ITAE can meet the control performance requirements. Among them, the initial value of the PI control parameter for the torque system calculated by the ITSE criterion has a short rise time. Still, the overshoot of the most important measurement index is 11%. However, the ITAE criterion can achieve 1% overshoot, and the adjustment time is relatively short. Therefore, the ITAE criterion with better all-around performance is selected to set the initial value K_p and K_i of PI control parameters for the torque system.

Based on the Routh method, the torque-speed systems at the other equilibrium points are identified. Then the initial value of PI control parameters for the torque system at the other equilibrium points can be calculated based on the ITAE.

IV. OPTIMIZATION OF CONTROL PARAMETERS AND CONSTRUCTION OF ADAPTIVE CONTROL

A. OPTIMIZATION OF CONTROL PARAMETERS

Since control parameters are inaccurate and the control objectives are difficult to coordinate by using traditional methods, it is necessary to optimize the PI control parameters of the torque system and active damping gain. In order to improve the control accuracy of generator speed and suppress the drive chain twist vibration, the Hierarchic Genetic Algorithm (HGA) is proposed to optimize the PI control parameters and active damping gains at each equilibrium point.

Compared with the other bionic algorithm, the Genetic Algorithm (GA) has the advantages of strong search ability and strong robustness. At the same time, GA is widely used because it has strong applicability and can be combined with other algorithms. With the development of the wind power industry, the accuracy of wind turbine control parameters is required to be higher and higher. However, GA has problems of poor population diversity and premature convergence in the late optimization stage. Therefore, when GA is used to optimize control parameters, the accuracy of control parameters often cannot meet the requirement.

However, compared with GA, the population is divided into many subpopulations in the proposed HGA method. Crossover and mutation probabilities are randomly selected for independent evolution of each subpopulation. Furthermore, the best individual is selected at the last stage of optimization, which can overcome the disadvantage of premature convergence and maintain population diversity. Moreover, it can also further improve the global and local search ability of the algorithm. Therefore, the control parameters with higher control accuracy can be obtained.

The main parameter value of the HGA is shown in Table 3 [25], [26]. Furthermore, the structure of HGA is shown in Figure 8.

TABLE 3. Main parameter value of the HGA.

Main parameter name	Main parameter value	Abbreviation
Population size	500	M=500
Subpopulation size	50	M_i=50
Number of subpopulations	10	N=10
Generations	100	G=10
Crossover probability	[0.7, 1)	P_c=[0.7, 1)
Mutation probability	(0, 0.3]	P_m=(0, 0.3]

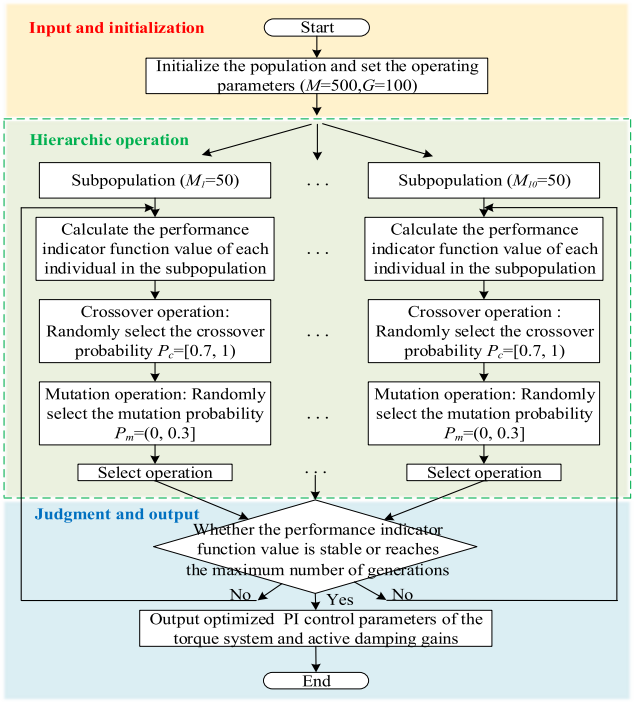

FIGURE 8. Structure of HGA.

The PI control parameters and active damping gains at each equilibrium point can be optimized based on HGA. The steps of the HGA algorithm are as follows.

First, the population is initialized, and the operating parameters are set. Since the wind turbine is the controlled system, the random seeds and turbulence intensities of turbulent winds are used as the input values. Moreover, the PI control parameters of the torque system and active damping gain K_p, K_i, and H_c are used as the initial values.

Secondly, the initialized population is equally divided into ten subpopulations. Each subpopulation size is selected as 50.

Thirdly, the performance indicator function values of each individual in subpopulations are calculated. The performance indicator function J_T is constructed by ITAE of the generator speed and the twist vibration of the drive chain. The performance indicator function J_T is shown in equation (13).

$$J_T = \xi \omega_g^{ITAE} + (1-\xi)(d\gamma/dt)^{ITAE} \tag{13}$$

where, ξ denotes the weight, ω_g^{ITAE} denotes the generator speed ITAE, $(d\gamma/dt)^{ITAE}$ denotes the drive chain twist rate ITAE. The variables in equation (13) can be expressed as:

$$\omega_g^{ITAE} = \int_0^{\infty} (t_{\omega_g} \left| e_{\omega_g}(t_{\omega_g}) \right|) dt \tag{14}$$

$$\omega_g^{ITAE} = \int_0^{\infty} (t_{\omega_g} \left| e_{\omega_g}(t_{\omega_g}) \right|) dt \tag{15}$$

where, t denotes time, $e(t)$ denotes the error function.

Next, crossover, mutation, and selection operations are carried out among individuals in each subpopulation. Crossover and mutation probabilities are randomly selected for each subpopulation within a specified range. Each individual evolves independently in its subpopulation.

Finally, the optimal individuals in each subpopulation are compared. Then the best individual in the whole population is selected, and the value of the performance indicator function is calculated. If the value of the performance indicator function is stable or reaches the maximum number of generations, the PI control parameters of the torque system and the drive chain active damping gain become the output values. If not, the algorithm enters the step of calculating the performance indicator function value of the individual in each subpopulation again.

The performance indicator function J_T constructed by ITAE is composed of two parts, which need to be allocated the weight. Therefore, the Pareto method is proposed to allocate the weight relationship between the two control objectives. The Pareto of the performance index function of wind speed 10 m/s is shown in Figure 9.

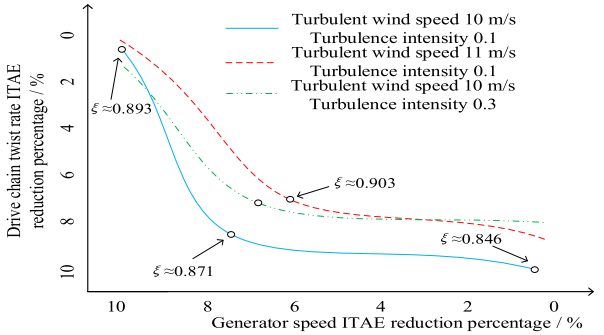

FIGURE 9. Pareto under different wind conditions.

Under the same wind condition, the generator speed and the drive chain twist rate ITAE all decreases when ξ changes within a specific range. With the increase of ξ, the generator speed ITAE decreases, but the drive chain twist rate ITAE increases. In contrast, under different wind condition, the optimal value ξ changes with wind speed v and turbulence intensity. When the turbulence intensity is 0.1, and the average wind speed is 10 m/s, it is considered that $\xi \approx 0.871$ is the optimal value at this time. When the turbulence intensity is 0.1, the relationship between optimal value ξ and wind speed can be expressed as:

$$\xi = 1 - \frac{129}{v^3} \tag{16}$$

Therefore, the weight in the performance index function is optimized by using Pareto. Since the PI control parameters and active damping gain K_p, K_i, and H_c of the $G_{10}(s)$ are optimized by HGA, the change curves in the performance indicator function J_T of the best individual in the population are shown in Figure 10.

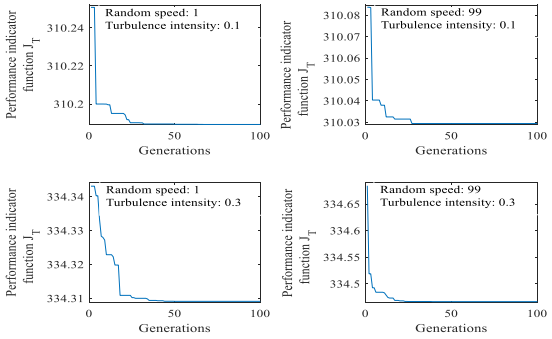

FIGURE 10. Change curves of performance indicator function.

According to the analysis, optimizing PI control parameters of the torque system and active damping gain based on HGA is closer to the object effect with the increase in population generations. The turbulent wind random seeds have little influence on the optimization results. It proves that optimized PI control parameters of the torque system and active damping gain have excellent control effect on different types of turbulent wind with the same intensity. Since the parameters of wind turbines have the time-varying characteristic, the optimization effect of PI control parameters of the torque system and active damping gain is relatively poor in the case of high turbulence intensity. Therefore, the PI control parameter and active damping gain corresponding to the turbulence intensity of 0.1 are selected, which are written as $K_p^{optimal}$, $K_i^{optimal}$, and,$H_c^{optimal}$.

Based on the proposed HGA and Pareto methods, the optimal value of the PI control parameters and active damping gains at other equilibrium points can be obtained.

B. CONSTRUCTION OF ADAPTIVE CONTROL

During torque control, the parameters of the wind turbine vary with wind speed. When the wind turbine operates far from the equilibrium points, the PI control parameters and active damping gains designed based on the equilibrium points cannot maintain the optimal control state [27]. At the same time, constant or discrete PI control parameters and active damping gains will result in unsatisfactory control effect. Therefore, a continuous adaptive control method of the torque system is proposed to solve the above problems. The proposed adaptive control is constructed by fitting the discrete PI control parameters of the torque system and the active damping gains with the wind speed. In order to ensure the control performance far from the equilibrium points, the PI control parameters of the torque system and active damping gains can be calculated and switched by adaptive control in real time under the turbulent wind. Thus, adaptive control can improve the robustness and stability of the control system. The adaptive control parameters of the torque system are shown in Table 4.

TABLE 4. Adaptive control parameters of the torque system.

Wind speed (m/s)	9	9.5	10	10.5	11
$K_p^{optimal}$	452	491	536	603	672
$K_i^{optimal}$	221	247	276	303	338
$H_c^{optimal}$	873	704	552	438	366

The least-square method is adopted to fit the discrete PI control parameters and active damping gain in Table 4 with the wind speed. The constructed continuous adaptive control can be expressed as:

$$K_p^{optimal}(v) = 26v^2 - 410v + 2036 \tag{17}$$

$$K_i^{optimal}(v) = 2.5v^2 + 7.5v - 49 \tag{18}$$

$$H_c^{optimal}(v) = 66.5v^2 - 1584.5v + 9747 \tag{19}$$

where, $K_p^{optimal}(v)$, $K_i^{optimal}(v)$, and $H_c^{optimal}(v)$ denote wind speed functions of proportional coefficient, integral coefficient, and active damping gain, respectively.

The Goodness of Fit of equations (17), (18), and (19) are 99.59%, 97.63%, and 98.92%, respectively, which meet the requirement of fitting accuracy. Therefore, the corresponding control parameters can be calculated and switched by the proposed adaptive control far from the equilibrium point. Analyzing equations (17), (18), and (19), the adaptive control curves are shown in Figure 11.

Analyzing Figure 11, the proposed continuous adaptive control method can maintain excellent control performance by calculating and switching control parameters far from the equilibrium points.

V. SIMULATION RESULTS

In order to verify the effectiveness of the proposed method, the 2MW wind turbine is built based on the Bladed software in this paper. Since the 2MW wind turbine is a nonlinear

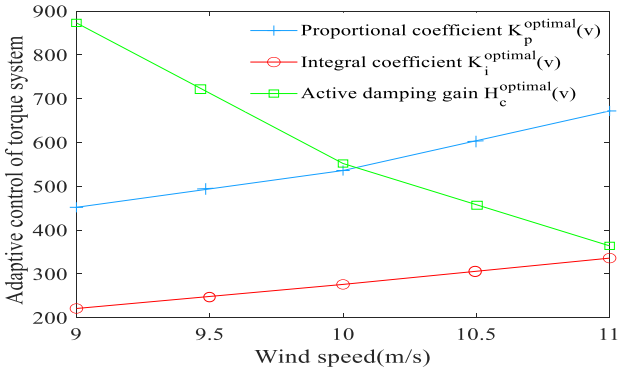

FIGURE 11. Adaptive torque control parameters curve.

system, the applicability of the proposed method can be verified according to the simulation results. Furthermore, by comparing control strategy 1, control strategy 2, and control strategy 3, the control effect of the proposed method can be verified. The meaning and abbreviation of the different control strategy is shown in Table 5.

TABLE 5. Meaning and abbreviation of the different control strategy.

Control strategy	Meaning	Abbreviation
Control strategy 1	The adaptive PI control of the torque system is based on initial values of control parameters.	PI
Control strategy 2	The adaptive PI control of the torque system and adaptive active damping control of the drive chain is based on initial values of control parameters.	PI+D
Control strategy 3	The adaptive PI control of the torque system and adaptive active damping control of the drive chain is based on optimal values of control parameters.	PI+D+OP

A. FREQUENCY-DOMAIN SIMULATION RESULTS

To verify the stability of the torque system after adding active damping control, the Bode plot of the torque system is shown in Figure 12.

Comparing control strategy 1 and 2, it can be observed from Figure 12 that the phase margin and amplitude margin are greater than zero. The phase and amplitude have a large stability margin, consequently. Therefore, the Bode plot shows that the torque system can maintain strong stability after adding the active damping control of the drive chain. Comparing control strategy 2 and 3, it can be observed from Figure 12 that the phase and amplitude are still greater than zero after optimizing the control parameters, which can guarantee the strong stability of the torque system.

To verify that the resonance frequency of the drive chain is in the desired range, the mode of the drive chain is analyzed. The Campbell diagram of the drive chain mode is shown

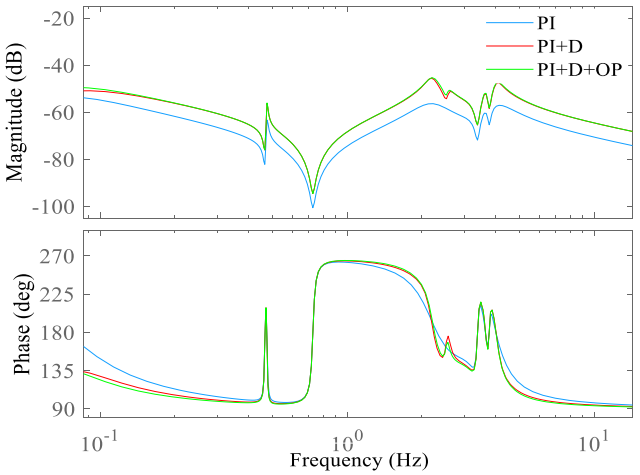

FIGURE 12. Bode plot of torque system.

in Figure 13 according to wind wheel speed and resonance frequency.

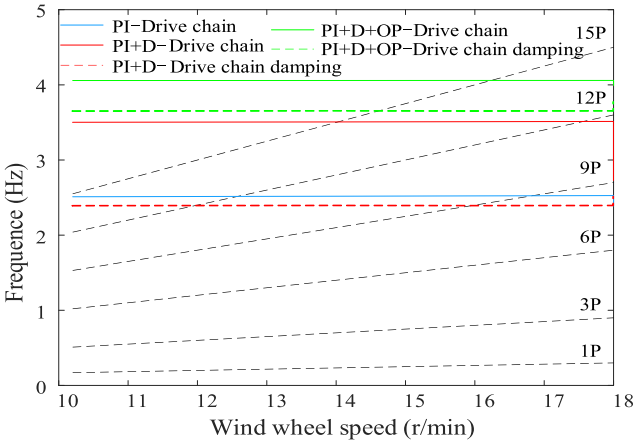

FIGURE 13. Campbell diagram of drive chain.

Comparing control strategy 1 and 2, it can be observed from Figure 13 that the resonance frequency of the drive chain can be changed from 2.52 Hz to 3.48 Hz after adding active damping control. The intersection between the drive chain resonance frequency of 3.48 Hz and the ninth-order natural frequency (9P) can be avoided, thereby avoiding resonance. At the same time, the resonance frequency of the drive chain damping can be obtained. Therefore, most of the drive chain resonance near 2.52 Hz will be undertaken by the drive chain damping. Comparing control strategy 2 and 3, by analyzing Figure 13, the resonance frequency of the drive chain and the drive chain damping can be changed by optimizing the control parameters. Therefore, the intersection between the resonance frequency and third-order (3P), sixth-order (6P), ninth-order (9P), and twelfth-order (12P) natural frequency can be avoided, thus preventing severe resonance.

To verify the ability of the proposed method to suppress the vibration of the drive chain, the self-power spectral density is

calculated based on the Fourier transform of the autocorrelation function. The self-power spectral density of the drive chain twist rate is shown in Figure 14.

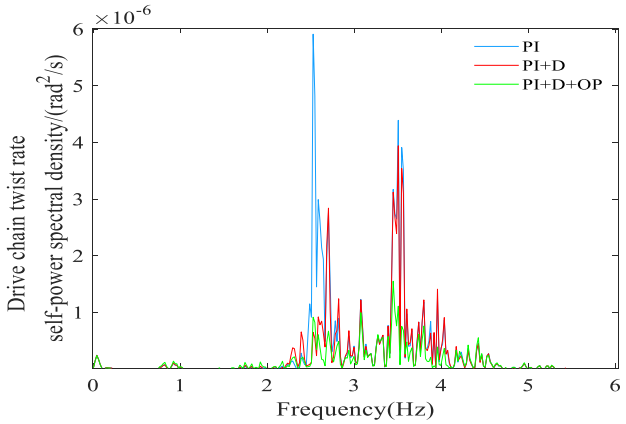

FIGURE 14. Self-power spectral density.

Comparing control strategy 1 and 2, by analyzing Figure 14, the component of the self-power spectral density of the drive chain twist rate is significantly decreased near 2.52 Hz. Therefore, the resonance of the drive chain near 2.52 Hz can be avoided when additional active damping control is used. Comparing control strategy 2 and 3, it can be observed from Figure 14 that the component of the self-power spectral density of the drive chain twist rate is significantly reduced near 2.52 Hz and 3.48 Hz, which shows that severe resonance of the drive train near 2.52 Hz and 3.48 Hz can be significantly avoided.

Analyzing Figure 12, 13, and 14, it can be found that the stability of the torque system can be ensured, and the twist rate of the drive chain near 2.52Hz and 3.48Hz can be significantly reduced. Furthermore, the drive chain and drive chain damping resonance with 3P, 6P, 9P, and 12P can be avoided after using the proposed method. Therefore, the proposed method is applicable.

B. TIME-DOMAIN SIMULATION RESULTS

(1) The analysis of control accuracy

A turbulent wind condition of 10 m/s is set according to the Kaimal model and International Electro technical Commission (IEC) standards, as shown in Figure 15. Since wind turbines under turbulent wind can be far from the equilibrium points at certain times, the applicability of the proposed method can be verified according to the simulation results.

The control effect of generator torque, output power, and generator speed under the wind speed of 10m/s are shown in Figure 16, 17, and 18.

Analyzing Figure 16, 17, and 18, the analysis results can be obtained as shown in Table 6.

According to the Germanischer Lloyd (GL) criterion and the steady curve of the 2MW wind turbine, the MEAN of generator torque, output power, and generator speed all satisfy the control requirements of wind turbines, which proves the applicability of the proposed method.

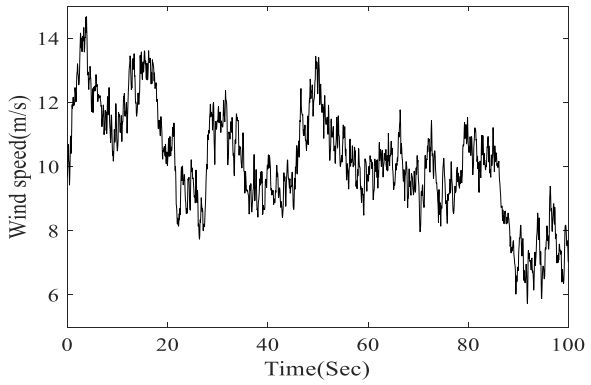

FIGURE 15. Turbulent wind condition of 10 m/s.

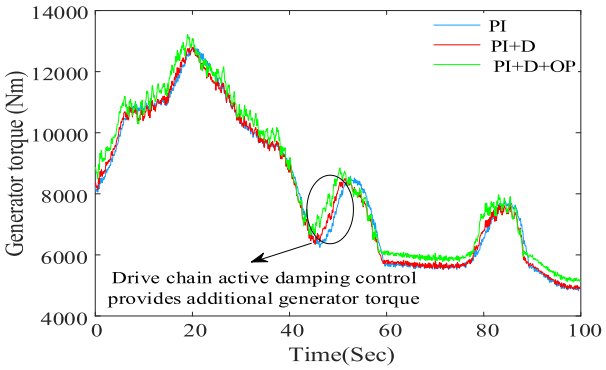

FIGURE 16. Variation curves of generator torque.

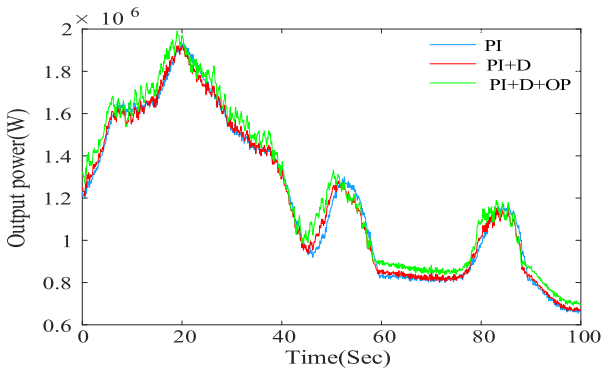

FIGURE 17. Variation curves of output power.

TABLE 6. Summary of performance indicators.

	Control strategy 1	Control strategy 2	Control strategy 3
Output power MEAN (W)	1.201×10^{6}	1.203×10^{6}	1.216×10^{6}
Output power RMSE	3.653×10^{5}	3.623×10^{5}	3.581×10^{5}
Generator speed RMSE	3.490×10^{1}	3.372×10^{1}	3.013×10^{1}

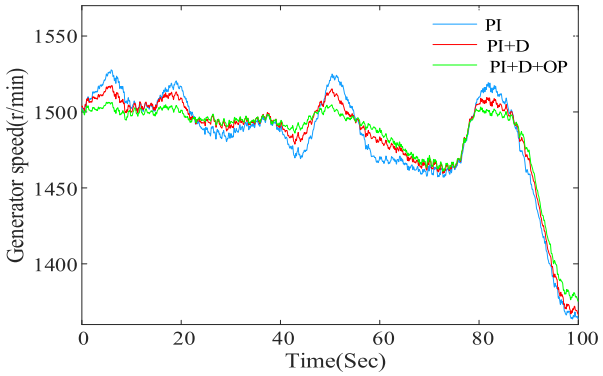

FIGURE 18. Variation curves of generator speed.

Comparing control strategy 1 and 2, the output power MEAN is increased by 0.17%, and the Root Mean Square Error (RMSE) is decreased by 0.82%. Moreover, the generator speed RMSE is also decreased by 3.38%. Comparing control strategy 2 and 3, the output power MEAN is increased by 1.08%, and the RMSE is decreased by 1.16%. Moreover, the generator speed RMSE is also decreased by 10.65%. The above results show that the output power can be increased, and the control accuracy of power and generator speed can be improved after using the proposed method. Therefore, the proposed method is applicable.

(2) The analysis of the drive chain twist vibration

In order to verify the vibration of the drive chain, the twist rate of the drive chain is shown in Figure 19.

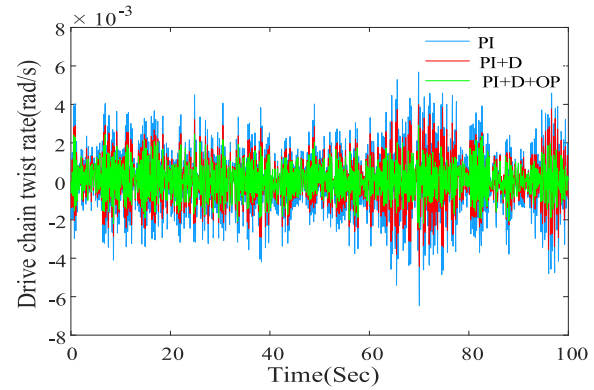

FIGURE 19. Variation curves of twist rate drive chain.

Analyzing Figure 19, the analysis results can be obtained as shown in Table 7.

Comparing control strategy 1 and 2, the twist rate of drive chain RANGE and MEAN are decreased by 35.52% and 13.36%, respectively. Comparing control strategy 2 and 3, the twist rate of drive chain RANGE and MEAN are decreased by 32.88% and 5.93%, respectively. The above results show that the twist vibration of the drive chain can be suppressed after using the proposed method. Therefore, the proposed method is applicable.

TABLE 7. Summary of performance indicators.

	Control strategy 1	Control strategy 2	Control strategy 3
Twist rate RANGE (rad/s)	0.125×10^{-1}	0.806×10^{-2}	0.541×10^{-2}
Twist rate MEAN (rad/s)	-1.984×10^{-5}	-1.719×10^{-5}	-1.617×10^{-5}

(3) The analysis of the tower top side-side vibration

In order to verify the side-side vibration of the tower top, the side-side velocity and acceleration are shown in Figure 20 and 21.

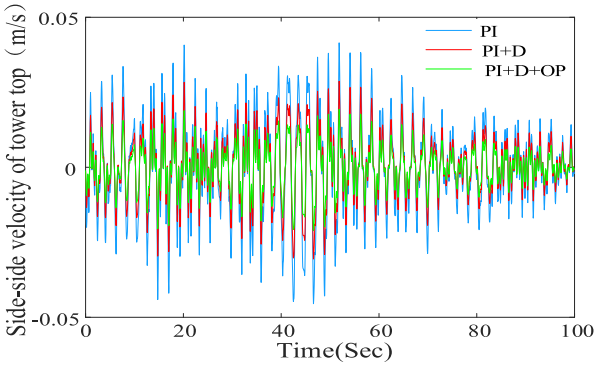

FIGURE 20. Variation curves of velocity side-side tower top.

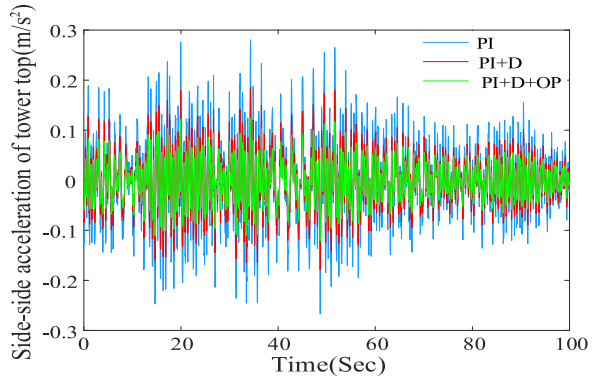

FIGURE 21. Variation curves of acceleration side-side tower top.

Analyzing Figure 20 and 21, the analysis results can be obtained as shown in Table 8.

Comparing control strategy 1 and 2, the side-side velocity RANGE and MEAN of the tower top are decreased by 33.84% and 6.56%. Moreover, the side-side acceleration RANGE and MEAN of the tower top are also decreased by 35.29% and 13.71%. Comparing control strategy 2 and 3, the side-side velocity RANGE and MEAN of the tower top are decreased by 27.15% and 1.36%. Moreover, the side-side

TABLE 8. Summary of performance indicators.

	Control strategy 1	Control strategy 2	Control strategy 3
Velocity RANGE (m/s)	0.863×10^{-1}	0.571×10^{-1}	0.416×10^{-1}
Velocity MEAN (m/s)	0.549×10^{-4}	0.513×10^{-4}	0.506×10^{-4}
Acceleration RANGE (m/s^2)	0.578×10^{0}	0.374×10^{0}	0.263×10^{0}
Acceleration MEAN (m/s^2)	-0.175×10^{-5}	-0.151×10^{-5}	-0.134×10^{-5}

acceleration RANGE and MEAN of the tower top are also decreased by 29.68% and 11.26%. The above results show that the side-side vibration of the tower top can be suppressed after using the proposed method. Therefore, the proposed method is applicable.

(4) The analysis of the tower bottom load

In order to verify the load of tower bottom, the Fy timing sequence load is shown in Figure 22.

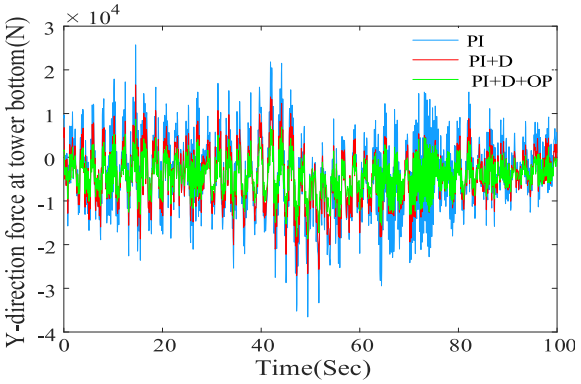

FIGURE 22. Variation curves of tower bottom y-direction force.

Analyzing Figure 22, the analysis results can be obtained as shown in Table 9.

TABLE 9. Summary of performance indicators.

	Control strategy 1	Control strategy 2	Control strategy 3
Fy RANGE (N)	6.774×10^{4}	4.239×10^{4}	2.914×10^{4}
Fy MEAN (N)	-3.731×10^{3}	-3.578×10^{3}	-3.509×10^{3}

The fatigue load is calculated based on the above timing sequence load and Weibull annual wind speed distribution. In addition, the fatigue load of the wind turbine is quantified by the Damage Equivalent Load (DEL), as shown in Table 10.

TABLE 10. Comparison of DEL at tower bottom.

	Control strategy 1	Control strategy 2	Control strategy 3
Fy DEL (N)	8.412×10^{4}	8.159×10^{4}	8.027×10^{4}

Comparing control strategy 1 and 2, the Fy timing sequence load RANGE and MEAN of the tower bottom are decreased by 37.42% and 4.10%, respectively. Therefore, the Fy DEL of the tower bottom is decreased by 3.01%. Comparing control strategy 2 and 3, the Fy timing sequence load RANGE and MEAN of the tower bottom are decreased by 31.26% and 1.93%, respectively. Therefore, the Fy DEL of the tower bottom is decreased by 1.62%. The above results show that the y-direction timing sequence load and DEL of the tower bottom can be decreased after using the proposed method. Therefore, the proposed method is applicable.

VI. CONCLUSION

Considering the mutual coupling effect of wind turbine control parameters, an optimization method of the control parameters for torque system based on drive chain active damping control is proposed, which improves the control accuracy and solves the problem that the control objectives are difficult to coordinate. The following conclusions can be drawn.

(1) Frequency-domain simulations: the proposed method is applicable. The sufficient stability margin of the torque system can be ensured. At the same time, the intersection between the resonance frequency and 6P, 9P, and 12P can be avoided, thus preventing severe resonance. Moreover, the component of the self-power spectral density of the drive chain twist rate is significantly reduced near the resonance frequency of the drive train.

(2) Time-domain simulations: the proposed method is applicable. The output power is increased, and the control accuracy of output power and generator speed is improved. Furthermore, the twist vibration of the drive chain, the side-side vibration of the tower top, and the Fy timing sequence load and Damage Equivalent Load of the tower bottom are decreased after using the proposed method.

In the future, the online optimization method to improve control accuracy according to real-time wind conditions will become a hot research topic. Therefore, the research on real-time online optimization methods of control parameters based on faster optimization speed and higher optimization accuracy is of great significance, which is our future research work.

APPENDIX I

In equation (1), A, B, C, and D denote three-dimensional coefficient matrices, x denotes the state variable; u and y

denote the input variable and output variable. Due to the complexity of the state space equation, only part of the state space equation is shown.

A is a $45 \times 45 \times 22$ matrix, and only the previous $7 \times 3 \times 1$ is taken as an example:

$$A = \begin{bmatrix} 0 & 0 & 0 \\ -0.0001 \times 10^5 & 0 & 0 \\ 0 & 0 & 0 \\ 0 & 0 & -0.0001 \times 10^5 \\ 0 & 0 & 0 \\ 0 & 0 & 0 \\ 0 & 0 & 0 \end{bmatrix} \quad \text{(I1)}$$

B is a $45 \times 3 \times 22$ matrix, and only the previous $7 \times 3 \times 1$ is taken as an example:

$$B = \begin{bmatrix} 0 & 0 & 0 \\ 0 & -0.0003 & 0 \\ 0 & 0 & 0 \\ 0.0162 & 0.0002 & 0 \\ 0 & 0 & 0 \\ 0 & 0 & 0 \\ 0 & 0 & 0 \end{bmatrix} \quad \text{(I2)}$$

C is a $12 \times 45 \times 22$ matrix, and only the previous $7 \times 3 \times 1$ is taken as an example:

$$C = \begin{bmatrix} 0 & 0 & 0 \\ 0 & 0 & 0 \\ 0 & 0 & 0 \\ 0 & 0 & 0 \\ 0 & 0 & 0 \\ 0 & 0 & 0 \\ -0.0865 \times 10^9 & -0.0003 \times 10^9 & 0 \end{bmatrix} \quad \text{(I3)}$$

D is a $12 \times 3 \times 22$ matrix, and only the previous $7 \times 3 \times 1$ is taken as an example:

$$D = \begin{bmatrix} 0 & 0 & 0.846 \times 10^3 \\ 0 & 0 & 0 \\ 0 & 0 & 0.001 \times 10^3 \\ 0 & 0 & 0 \\ 0 & 0 & 0 \\ 0 & 0 & 0 \\ -0.0137 \times 10^3 & -0.1039 \times 10^3 & -0.0010 \times 10^3 \end{bmatrix} \quad \text{(I4)}$$

TABLE 11. Part state variables.

	State variables
1	Tower displacement mode 1
2	Tower velocity mode 1
3	Tower acceleration mode 1

TABLE 12. Input variables.

	Input variables
1	Wind speed
2	Pitch angle demand
3	Generator torque demand

x contains 45 state variables. Only the previous three are taken as an example:

TABLE 13. Part output variables.

	Output variables
1	Measured power
2	Measured generator speed
3	Generator torque

ACKNOWLEDGMENT

The authors would like to thank Shenyang Huaren Wind Power Technology Company Ltd., for providing wind turbine data and test platform.

REFERENCES

[1] R. You and X. Lu, "Voltage unbalance compensation in distribution feeders using soft open points," *J. Mod. Power Syst. Clean Energy*, vol. 10, no. 4, pp. 1000–1008, Jul. 2022.
[2] X. Deng, J. Yang, Y. Sun, D. Song, Y. Yang, and Y. H. Joo, "An effective wind speed estimation based extended optimal torque control for maximum wind energy capture," *IEEE Access*, vol. 8, pp. 65959–65969, 2020.
[3] L. Rosado, J. Samanes, E. Gubia, and J. Lopez, "Robust active damping strategy for DFIG wind turbines," *IEEE Trans. Power Electron.*, vol. 36, no. 12, pp. 14525–14538, Dec. 2021.
[4] H. M. M. Adil, S. Ahmed, and I. Ahmad, "Control of MagLev system using supertwisting and integral backstepping sliding mode algorithm," *IEEE Access*, vol. 8, pp. 51352–51362, 2020.
[5] Z. Wu, G. Zhang, W. Du, J. Wang, F. Han, and D. Qian, "Torque control of bolt tightening process through adaptive-gain second-order sliding mode," *Meas. Control*, vol. 53, nos. 7–8, pp. 1131–1143, Jul. 2020.
[6] R. You, X. Yuan, and X. Li, "A multi-rotor medium-voltage wind turbine system and its control strategy," *Renew. Energy*, vol. 186, pp. 366–377, Mar. 2022.
[7] K. T. Sundari, C. Komathi, S. Durgadevi, and K. Abirami, "Optimal controller tuning of a PI controller for a three tank non-interacting process," in *Proc. Int. Conf. Power, Energy, Control Transmiss. Syst. (ICPECTS)*, Chennai, India, Dec. 2020, pp. 1–5.
[8] J. Shair, X. Xie, J. Yang, J. Li, and H. Li, "Adaptive damping control of subsynchronous oscillation in DFIG-based wind farms connected to series-compensated network," *IEEE Trans. Power Del.*, vol. 37, no. 2, pp. 1036–1049, Apr. 2022.
[9] W. He, "A generic understanding of damping effect of wind power generation with inertial response on synchronous generator," in *Proc. IEEE 4th Int. Electr. Energy Conf. (CIEEC)*, Wuhan, China, May 2021, pp. 1–5.
[10] A. Gambier and A. Behera, "Integrated pitch control system design of a wind turbine by using multiobjective optimization," *IFAC-PapersOnLine*, vol. 51, no. 28, pp. 239–244, 2018.
[11] X. Zhou, J. Zhou, C. Yang, and W. Gui, "Set-point tracking and multi-objective optimization-based PID control for the goethite process," *IEEE Access*, vol. 6, pp. 36683–36698, 2018.
[12] F. Gao, X. M. Ling, and W. Wang, "PI parameters joint tuning for individual pitch controller of large wind turbine," *Acta Energiae Solaris Sinica*, vol. 3, no. 2, pp. 307–314, Feb. 2018.
[13] S. Wang, H. Liang, and J. Wang, "GA PID control research in inverter motor speed governing system," *J. Comput. Methods Sci. Eng.*, vol. 19, no. 2, pp. 299–306, May 2019.
[14] Z. Long, Z. Jiang, C. Wang, Y. Jin, Z. Cao, and Y. Li, "A novel approach to control of piezo-transducer in microelectronics packaging: PSO-PID and editing trajectory optimization," *IEEE Trans. Compon., Packag., Manuf. Technol.*, vol. 10, no. 5, pp. 795–805, May 2020.
[15] Y. Sun, J. Xu, G. Lin, and N. Sun, "Adaptive neural network control for maglev vehicle systems with time-varying mass and external disturbance," *Neural Comput. Appl.*, vol. 2021, pp. 1–12, Mar. 2021, doi: 10.1007/S00521-021-05874-2.
[16] A. Al Zawaideh and I. M. Boiko, "Analysis of stability and performance of a cascaded PI sliding-mode control DC–DC boost converter via LPRS," *IEEE Trans. Power Electron.*, vol. 37, no. 9, pp. 10455–10465, Sep. 2022.

[17] A. Iqbal, D. Ying, A. Saleem, M. A. Hayat, and M. Mateen, "Proposed particle swarm optimization technique for the wind turbine control system," *Meas. Control*, vol. 53, nos. 5–6, pp. 1022–1030, Feb. 2020.
[18] *GH Bladed: Theory Manual*, Garrad Hassan and Partners Ltd., Beijing, China, 2012.
[19] S. Jiang, R. Lv, L. Wan, Q. Mao, Q. Zeng, K. Gao, and Y. Yang, "Dynamic characteristics of the chain drive system of scraper conveyor based on the speed difference," *IEEE Access*, vol. 8, pp. 168650–168658, 2020.
[20] Z.-X. Xing, L.-Z. Liang, H.-Y. Guo, and X.-D. Wang, "Damping control study of the drive train of DFIG wind turbine," in *Proc. Int. Conf. Energy Environ. Technol.*, Guilin, China, 2009, pp. 576–579.
[21] J. Licari, C. E. Ugalde-Loo, J. B. Ekanayake, and N. Jenkins, "Damping of torsional vibrations in a variable-speed wind turbine," *IEEE Trans. Energy Convers.*, vol. 28, no. 1, pp. 172–180, Mar. 2013.
[22] L. Y. Shao, "Optimal control on active damping load reduction for key bearing components of large wind turbines," *Sci. Technol. Eng.*, vol. 20, no. 20, pp. 8193–8201, Oct. 2020.
[23] S. K. Gautam, S. Nema, and R. K. Nema, "Model order reduction of interval systems using Routh approximation with mid-point concept and stability equation method," in *Proc. IEEE 2nd Int. Conf. Electr. Power Energy Syst. (ICEPES)*, Bhopal, India, Dec. 2021, pp. 1–5.
[24] R. Buchi, "Optimal ITAE criterion PID parameters for PTn plants found with a machine learning approach," in *Proc. 9th Int. Conf. Control, Mechatronics Autom. (ICCMA)*, Belval, Luxembourg, Nov. 2021, pp. 50–54.
[25] Q. Zhu and Y. Zhang, "Parallel machine scheduling problem based on improved hierarchic genetic algorithm," in *Proc. 36th Youth Academic Annu. Conf. Chin. Assoc. Autom. (YAC)*, Nanchang, China, May 2021, pp. 266–270.
[26] X. Yan, C. Duan, X. Chen, and Z. Duan, "Planning of electric vehicle charging station based on hierarchic genetic algorithm," in *Proc. IEEE Conf. Expo Transp. Electrific. Asia–Pacific*, Beijing, China, Aug. 2014, pp. 1–5.
[27] Y. Sun, J. Xu, C. Chen, and W. Hu, "Reinforcement learning-based optimal tracking control for levitation system of maglev vehicle with input time delay," *IEEE Trans. Instrum. Meas.*, vol. 71, pp. 1–13, 2022.

YINGMING LIU was born in Liaoning, China, in 1973. He received the B.S. degree in applied electronic technology, the M.S. degree in electrical engineering, and the Ph.D. degree in electrical theory and new technology from the Shenyang University of Technology. He is currently a Professor with the Shenyang University of Technology. His research interests include new energy power generation, new energy grid connection, and coordination of wind-storage combination.

SHUYUAN ZHANG was born in Luoyang, Henan, China, in 1998. He received the B.S. degree in electrical engineering from the Zhengzhou University of Aeronautics, Zhengzhou, China, in 2020. He is currently pursuing the M.S. degree in electrical engineering with the Shenyang University of Technology, Shenyang, China. His research interests include wind turbine control technology, intelligent optimization of control parameters, and intelligent algorithms.

XIAODONG WANG was born in Henan, China, in 1978. He received the B.S. and M.S. degrees in computer science and the Ph.D. degree in electrical theory and new technology from the Shenyang University of Technology, Liaoning, Shenyang. He is currently a Professor with the Shenyang University of Technology. His research interests include wind power generation, big data analytics, and machine learning techniques.

XING GAO was born in Liaoning, China, in 1998. He received the B.S. degree in electrical engineering and automation from the Shenyang University of Technology, in 2018, where he is currently pursuing the Ph.D. degree in electrical engineering. His research interests include offshore wind farms fault diagnosis, machine learning techniques, and intelligent power prediction of offshore wind farms.

TIAN CAO was born in Puyang, Henan, China, in 1998. He received the B.S. degree in electrical engineering from the Zhengzhou University of Aeronautics, Zhengzhou, China, in 2020. He is currently pursuing the M.S. degree in electrical engineering with the China University of Mining and Technology, Xuzhou, China. His current research interests include stability analysis and control technology of the grid-connected inverter.